NANOSTRUCTURED PHOTOCATALYSTS

CHAPTER 3: ADVANCES IN PHOTOCATALYTIC MATERIALS FOR CO_2 REDUCTION APPLICATIONS

1. Introduction

Nanoscale materials usually exhibit unique physicochemical characteristics which differ greatly from their bulk counterparts (Jacobson, 2009; Faunce et al., 2013; Lin et al., 2014). Nanomaterials are normally fabricated in the form of Nanotubes (NTs), nanoparticles (NPs) and nanofibres (NFS). Apart from nanomaterials' exotic topologies (e.g., nanoflowers and nanobelts), nanomaterials usually possess high surface areas, distinct electronic states and tunable architectures (Luthi et al., 2008; Barber & Tran, 2013; Jia et al., 2012). Photocatalytic nanostructures particularly exist as thin-walled structures with high-density photoactive surfaces which are usually responsible for rapid transport of interfacial charge carriers to the adsorbates (Indrakanti et al., 2009; Morris et al., 2009; Varghese et al., 2009). For several years, carbon dioxide reduction has mainly depended on titania-based photocatalytic materials which only utilize a small fraction of the solar radiation spectra (i.e., 2%, typically as UVA) (Paracchino et al., 2011; Habisreutinger et al., 2013; Ma et al., 2014). Moreover, titania-based photocatalysts usually require study of doping or quantum effects for carrying out the reduction in their intrinsic bandgap values (Dau et al., 2010; Moore & Brudvig, 2011; Nocera, 2012). Combination of organic or inorganic supramolecular sensitizers (biomimetics) can be employed for enhancing the bandgap reduction capability of titania photocatalysts (Duan et al., 2012; Liu et al., 2012; Tahir & Amin, 2013). Significant developments in artificial photosynthesis have been realized by exploring photocatalytic nano-architectures, e.g. the breakthroughs in 'self-repairing' Co_xPO_4 catalysts generating O_2 (similar to natural manganese catalyst in a photosystem), development of TiO_2 based corrosion resistant nanocomposites for water-splitting, water-assisted reduction of CO_2 to yield olefins and CH_4, and the utilization of polymeric nitrides and metal oxynitrides for efficient water splitting applications under visible light (Ardo & Meyer, 2009; Reece et al., 2011; Handoko et al., 2013). Solar methane (CH_4) production from carbon dioxide has seen remarkable advancements in recent years, with titania nanotubes transporting hydrocarbons from 1 bar carbon dioxide CO_2 under sunlight at the rate of approximately 17.5 nanomoles $h^{-1}\,cm^{-2}\,mW^{-1}$ with roughly 0.74% quantum efficiency as defined below:

$$\eta = \frac{\Sigma_i M_i n_i}{P_m}$$

Where M_i denotes the mols of product i, P_m represents the mols of incident photons, and n_i is the number of electrons taking part in the generation of product I (Smith & Nie, 2009; Xi et al., 2012; Huang et al., 2014). Deposition of copper-doped titania coatings on solid substrates has been reported to deliver methane at the rate of 117 nanomoles h^{-1} cm^{-2} mW^{-1} (Liu et al., 2011; Yui et al., 2011; Liao et al., 2014). Key considerations for stability and photocatalytic corrosion resistance in various photocatalysts include quantum efficiency, selectivity and productivity towards hydrocarbons and synthesis routes for incorporation of photocatalysts into reactor designs to achieve efficient light absorption along with excellent mass transport (Yang et al., 2010; Feng et al., 2011; Izumi et al., 2013).

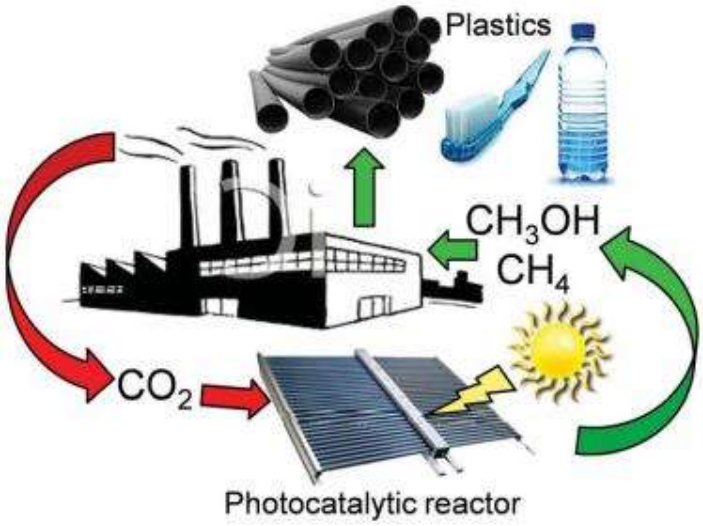

Fig. 14. Schematic illustration of a carbon zero route for renewable olefins and solar fuels through the reduction of CO_2 by photocatalysis

[Source: http://pubs.rsc.org/en/content/articlelanding/2015/ta/c5ta01592h]

2. Role of Crystallinity and engineered surface defects

The catalytic performance of photocatalysts is inherently linked to the electronic/optical characteristics of their surface. Additionally, the performance of photocatalysts also depends on adsorption characteristics of a photocatalyst surface which can be systematically regulated through crystal structure maneuvering (Inoue et al., 1979; Eggins et al., 1988; Roy et al., 2010). Crystallographic nature, uniformity, crystal phase termination and crystal dimensions strongly influence the photocatalytic efficiency of a particular photocatalyst. For example, the monoclinic sheet-like structure of $BiVO_4$ substantially outperforms tetragonal rod-like structured $BiVO_4$ (in the sense of photoreduction rates) for reduction of CO_2 to C_2H_5OH (followed by O_2 generation), under both visible and UV light illumination in an aqueous media. These tetragonal and monoclinic phases are obtained by the

introduction of cetyltrimethylammonium bromide (i.e., CTAB) or polyethylene glycol (i.e., PEG) during synthesis of $BiVO_4$ (Kuznetsov & Edwards, 2010; Kubacka et al., 2012; Tong et al., 2012). The superior photoactive performance of the monoclinic $BiVO_4$ is attributed to the asymmetric local atmosphere of the Bi3+ ions comparative to those present within the tetragonal phase. Accordingly, stronger lone pair characteristics are exhibited by the Bi^{3+} ions in the monoclinic phase which are responsible for Bi–O bond formation with CO_2 in the form of carbonates followed by subsequent photogenerated electronic transport from the V 3d band into the chemisorbed carbonate ions (CO_3^{-2}). It has been reported that these two distinct phases exhibit different UV-Vis absorption characteristics with the bandgap values of 2.56 eV and 2.24 eV for tetragonal and monoclinic $BiVO_4$, respectively. Recently, Li et al. (2013) illustrated the effectivity of cubic $NaNbO_3$ over orthorhombic $NaNbO_3$ for photoreduction of CO_2. The cubic $NaNbO_3$ (i.e., c-$NaNbO_3$) is usually stable at temperatures above 813 K. The synthesis of $NaNbO_3$ can be carried out via FAPO (i.e., furfural alcohol derived polymerization-oxidation) approach in the presence a surfactant stabilizer known as P123. Polymerized complex (PC) technique is typically employed for fabrication of orthorhombic $NaNbO_3$ (i.e., o-$NaNbO_3$) phase which is a more common phase of $NaNbO_3$. Structure of a typical c-$NaNbO_3$ is normally comprised of cuboid morphologies while a blend of the cuboid and irregular particles is observed for o-$NaNbO_3$. Both $NaNbO_3$ crystal phases exhibit analogous crystallite sizes (i.e., o-$NaNbO_3$ =23.1 nm versus c-$NaNbO_3$ = 18.5 nm) and surface areas (i.e., o-$NaNbO_3$ = 26.4 $m^2\ g^{-1}$ versus c-$NaNbO_3$ = 28.6 $m^2\ g^{-1}$) while the band gap of o-$NaNbO_3$ (3.45 eV) is generally greater than that of c-$NaNbO_3$ (3.29 eV). Under irradiation of UV light (Xe arc lamp of 300 W) in the presence of water vapors and a platinum co-catalyst, c-$NaNbO_3$ generates CH_4 (0.486 μmol h^{-1}) which is almost double the amount generated by o-$NaNbO_3$ (0.245 μmol h^{-1}) in a closed circulation gaseous system pressurized with CO_2 at 80 kPa. Calculations of density functional theory (DFT) are used to demonstrate this disparity in photocatalytic performance caused by the difference in conduction band energies and octahedral ligand fields. Accordingly, an efficient electronic excitation and transport mechanism observed for high symmetry phase (c-$NaNbO_3$) as compared to o-$NaNbO_3$ phase. In addition to H_2 (0.71 μmol h^{-1}) and CO_2 (0.082 μmol h^{-1}), trace amounts of C_2H_6, C_3H_8, and C_2H_4 are usually detected during photocatalysis of CO_2 over the c-$NaNbO_3$.

3. Nano-Synthesis Routes

Several synthesis routes (approaches) have been established for development of nanomaterials with manageable crystal facets, e.g., pH regulation of the fabrication media, post-synthesis treatments, etc. Truong et al. (2012) selectively synthesized TiO_2 based anatase (3% rutile, pH 2), rutile (6% of anatase, pH 6) and composite (pH 10) with 73% bi-crystalline anatase and 27% brookite composite. Under visible light or UV light (500 W Xe lamp) irradiation using the $NaNO_2$ solution as an ultraviolet cut-off filter in a $NaHCO_3$ solution, the above-mentioned materials exhibit photoreduction behavior of CO_2 to CH_3OH. The order of the photoactivity follows the pattern as indicated below:

Brookite-anatase composite > rutile phase > anatase phase > commercial P25. Liu et al. (2012) also successfully synthesized three different nanoarchitectures of TiO_2 based substances including, rutile (TiR) nano ellipses, brookite (TiB) nanorods and anatase (TiA) nanoparticles for photoreduction of CO_2 by exposing the as-synthesised TiO_2 to thermal treatment under a helium environment at a temperature of 220 ^{0}C for 1.5 hours to induce surface defects which include the inclusion of Ti^{3+} ions and oxygen vacancies (V_O) on TiO_2 polymorphs. Irradiation by a 150 Watt solar simulator in the presence of water vapors and CO_2 unveiled the polymorphs of TiO_2 as active components for photoreduction of CO_2 to CO and a trace amount of CH_4 under incessant-flow (i.e., 2.0 mL min^{-1}). Product yields exhibited a decrease in the following order:

TiA > TiB > TiR

As illustrated in Fig. 15, helium-treated materials (TiB (He and TiA (He)) considerably outperform their untreated counterparts, with the highest photoactivity exhibited by TiB (He) followed by relatively lower photoactivity shown by TiA (He). On the contrary, TiR shows lesser photoactive impacts as compared to other (helium treated) polymorphs of TiO_2 due to the presence of higher activation barriers to the creation of surface oxygen vacancies.

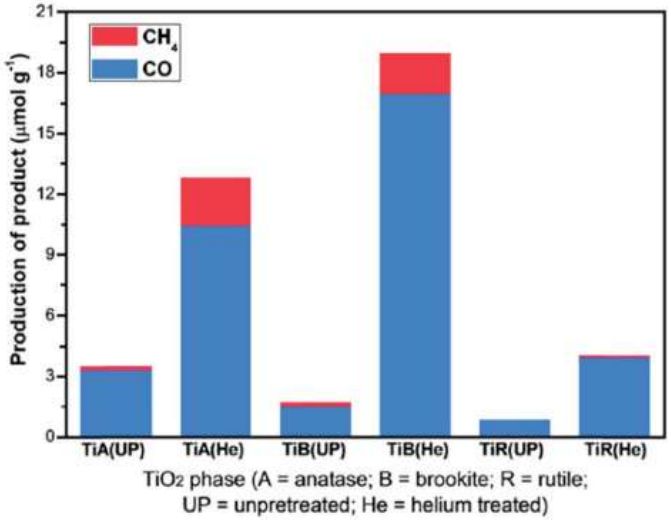

Fig. 15. CO and CH4 yield from He-treated and untreated TiO2 polymorphs during 6 hours irradiation under 150 Watt solar simulator in the existence of H2O vapors and CO2 in an incessant-flow photoreactor functioning at a flow rate of about two mL min^{-1}.

[Source: http://pubs.rsc.org/en/content/articlelanding/2015/ta/c5ta01592h]

In situ experiments have suggested that the relative oxygen vacancies and Ti^{3+} ions concentration in TiB (He) are comparable to that of TiA (He) while the concentration of surface defects on TiR (He) surface is negligible. The higher photoactivity of TiA (He) and TiB (He) is thus ascribed to surface defects. The vacancy formation energy for TiB (He) is typically 5.52 eV which is relatively lower than that of rutile

(5.82 eV) and anatase (5.58 eV). Photoreduction of CO_2 over TiO_2 is evidently a strong function of the surface defect density and crystal structure.

4. Effect of Crystal Facets on Photocatalysis

Extensive research has been conducted to investigate the effect of crystal facets on photocatalysis systems. Chemical and physical properties of single crystals are susceptible to crystallographic interruption (Yang et al., 2008; Liu et al., 2009; Yu et al., 2014). Calculations have proved that the average surface energy of low-indexed anatase facets declines in the order 0.90 J m^2 > 0.53 J m^2 > 0.44 J m^2 for (100), (001) and (101) facets, respectively (Lazzeri et al., 2001). The highest energy surface (001) is estimated to be the most reactive, and certain experimental studies certify that water and methanol undergo dissociative molecular adsorption on the (001) surface (Vittadini et al., 1998; Gong & Selloni, 2005). Consequently, efforts to regulate the morphological features of titania have focused on the production of nanostructures favorably exposing (001) facets or co-exposing (101) and (001) facets to improve dye degradation and water splitting (Wu et al., 2008; Yu et al., 2010; Wang et al., 2012).

Some other studies have reported that photooxidation and photoreduction activities follow the order as shown below:

(001) < (101) < (010)

(010) facet exhibits the superior performance because of the synergy between the electronic band structure (showing the CB potential) and surface atomic structure (showing dictating reactivity/adsorption).

Nanorods of TiO_2 favorably exposing (010) facets are typically screened in Photoreduction of CO_2 (Barpuzary et al., 2011). Such nanorods are produced by hydrothermal treatment of precursor $H_{0.68}Ti_{1.83}O_3$ in the presence of a pH mediator (Cs_2CO_3) followed by the subsequent promotion by one weight% platinum. The resulting platinum-doped titania nanorods outperform P25 in photoreduction of CO_2 to CH_4 by water vapors under UV irradiation of 300 W Xe lamp in a Teflon-lined steel chamber at 0.06 MPa CO_2 pressure. The enhanced photoactivity of titania nanorods is ascribed to the unique characteristics of (010) facets which facilitate CO_2 adsorption due to the presence of more negative potential in the conduction band (Indrakanti et al., 2008).

Hollow anatase single crystals and hollow anatase mesocrystals were reportedly produced by Indrakanti et al. (2008) and Jiao et al. (2012) which demonstrated the dominance of (101) facets in both nanostructures. These materials were successfully fabricated by hydrothermal treatment of a Na_3PO_4 and Ti $(SO_4)_2$ in HF solution. Fig. 16 (A–D) illustrates the resultant octahedral single crystals (400 nm diameter) developed using 500 mM HF. Decreasing the concentration of HF to 400 mM results in hollow crystals (~160 nm) with less distinct octahedral shapes (Fig. 16B & Fig. 16E). Fig. 16H

illustrates that these hollow crystals are principally (101) oriented single crystals with a small fraction of higher-index facets, i.e., (103) facets. Lower concentrations of HF also favor hollow (sphere-like) cages with 150 nm diameter (Fig. 16C and Fig. 16F). Each hollow (sphere-like) cage is developed from octahedral crystals (35 nm) which spontaneously self-organize during the process of crystal growth to assume a common crystallographic orientation, ultimately yielding 'single crystal-like' mesocrystals having well-defined selected area electron diffraction (or SAED) patterns.

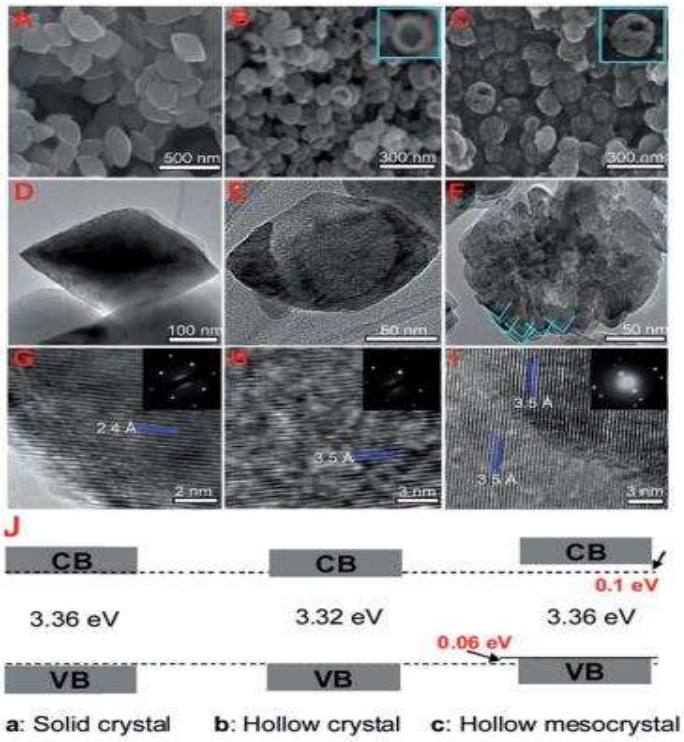

Fig. 16. (A–C) SEM images; (D-F) TEM images; (G–I) HRTEM images and (J) electronic band architectures based on valence band and UV-Vis XPS spectra of single crystal TiO_2 (solid anatase), single crystal hollow anatase, and hollow anatase monocrystals. Insets in (B) and (C) display hollow cores present in the single particles and mesocrystal particles; insets in (G, H and I) exhibit SAED patterns for the anatase TiO_2 based solid, hollow and hollow-meso single crystals

[Source: http://pubs.rsc.org/en/content/articlelanding/2015/ta/c5ta01592h]

Under UV illumination (300 Watt Xe lamp) and in the existence of water vapors and a co-catalyst (RuO_2), the hollow mesocrystal and single crystal titania outperform non-porous single crystals by a factor of roughly 4–5 times in photoreduction of CO_2 to CH_4. Higher photoreduction efficiencies of titania hollow crystal and mesocrystals are attributed to their following characteristics:

(i) Higher surface areas (35 $m^2\ g^{-1}$ for hollow crystals and 42 $m^2\ g^{-1}$ for hollow mesocrystals, respectively) as compared to the solid crystal with a surface area of 17 $m^2\ g^{-1}$

(ii) Suppressed bulk recombination and shorter diffusion lengths of charge carriers

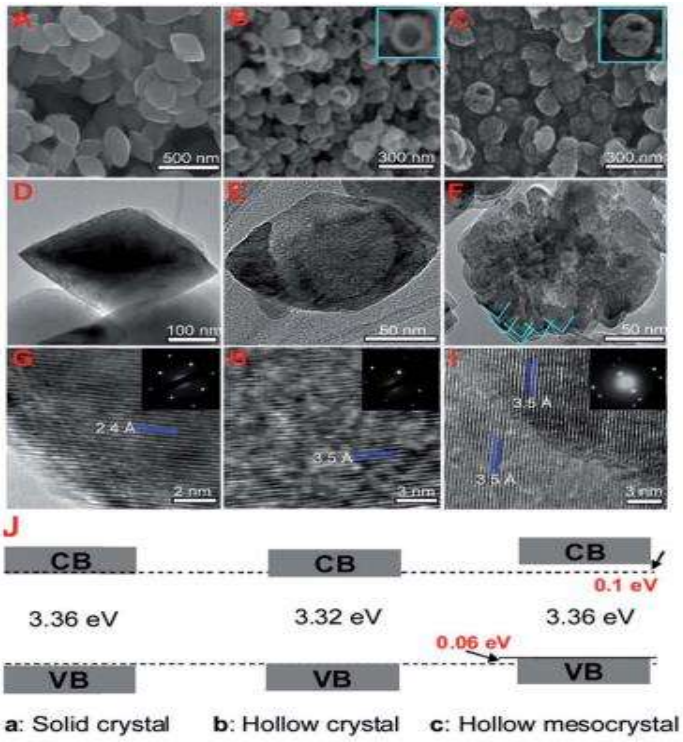

Fig. 17. (A–C) SEM images; (D-F) TEM images; (G–I) HRTEM images and (J) electronic band architectures based on valence band and UV-Vis XPS spectra of single crystal TiO_2 (solid anatase), single crystal hollow anatase, and hollow anatase monocrystals. Insets in (B) and (C) display hollow cores present in the single particles and mesocrystal particles; insets in (G, H and I) exhibit SAED patterns for the anatase TiO_2 based solid, hollow and hollow-meso single crystals.

[Source: http://pubs.rsc.org/en/content/articlelanding/2015/ta/c5ta01592h]

Fig. 17 demonstrates different electronic band architectures for titania based single crystals, single hollow crystals, and hollow mesocrystals along with the illustration of negative CB potential exhibited by hollow mesocrystals. Adsorbate-induced reformation of highly reactive crystal facets remains an inherent problem due to the presence of high surface energies. Therefore, reagents like isopropanol and HF have been employed as structure-regulating agents to favor the maximum exposure of (001) facets over single-crystal nanosheets of anatase (Liu et al., 2004). Utilization of such capping agents is also a challenging job since they need to be eliminated by thermochemical treatment before photocatalytic application (e.g., calcination or solvent extraction) which in turn may cause phase changes/surface restructuring. Synthesis of uniform and stable nanostructures terminating in particular atomic rearrangements necessitates continued development (Liu et al., 2010; 2011; 2012; 2013).

References

[1] Ardo, S., & Meyer, G. J. (2009). Photodriven heterogeneous charge transfer with transition-metal compounds anchored to TiO 2 semiconductor surfaces. *Chemical Society Reviews*, *38*(1), 115-164.

[2] Barber, J., & Tran, P. D. (2013). From natural to artificial photosynthesis. *Journal of The Royal Society Interface*, *10*(81), 20120984.

[3] Barpuzary, D., Khan, Z., Vinothkumar, N., De, M., & Qureshi, M. (2011). Hierarchically grown urchinlike CdS@ ZnO and CdS@ Al2O3 heteroarrays for efficient visible-light-driven photocatalytic hydrogen generation. *The Journal of Physical Chemistry C*, *116*(1), 150-156.

[4] Dau, H., Limberg, C., Reier, T., Risch, M., Roggan, S., & Strasser, P. (2010). The mechanism of water oxidation: from electrolysis via homogeneous to biological catalysis. *ChemCatChem*, *2*(7), 724-761.

[5] Duan, J., Shi, W., Xu, L., Mou, G., Xin, Q., & Guan, J. (2012). Hierarchical nanostructures of fluorinated and naked Ta 2 O 5 single crystalline nanorods: hydrothermal preparation, formation mechanism and photocatalytic activity for H 2 production. *Chemical Communications*, *48*(58), 7301-7303.

[6] Eggins, B. R. (1988). JTS Irvine, EP Murphy and J. Grimshaw. *J. Chem. Soc. Chem. Commun*, *1123*.

[7] Faunce, T., Styring, S., Wasielewski, M. R., Brudvig, G. W., Rutherford, A. W., Messinger, J., & Hankamer, B. (2013). Artificial photosynthesis as a frontier technology for energy sustainability. *Energy & Environmental Science*, *6*(4), 1074-1076.

[8] Feng, X., Sloppy, J. D., LaTempa, T. J., Paulose, M., Komarneni, S., Bao, N., & Grimes, C. A. (2011). Synthesis and deposition of ultrafine Pt nanoparticles within high aspect ratio TiO 2 nanotube arrays: application to the photocatalytic reduction of carbon dioxide. *Journal of Materials Chemistry*, *21*(35), 13429-13433.

[9] Gong, X. Q., & Selloni, A. (2005). Reactivity of anatase TiO2 nanoparticles: the role of the minority (001) surface. *The Journal of Physical Chemistry B*, *109*(42), 19560-19562.

[10] Habisreutinger, S. N., Schmidt-Mende, L., & Stolarczyk, J. K. (2013). Photocatalytic reduction of CO2 on TiO2 and other semiconductors. *Angewandte Chemie International Edition*, *52*(29), 7372-7408.

[11] Handoko, A. D., Li, K., & Tang, J. (2013). Recent progress in artificial photosynthesis: CO2 photoreduction to valuable chemicals in a heterogeneous system. *Current Opinion in Chemical Engineering*, *2*(2), 200-206.

[12] Huang, H., Wang, S., Zhang, Y., & Chu, P. K. (2014). Band gap engineering design for construction of energy-levels well-matched semiconductor heterojunction with enhanced visible-light-driven photocatalytic activity. *RSC Advances*, *4*(78), 41219-41227.

[13] Indrakanti, V. P., Kubicki, J. D., & Schobert, H. H. (2008). Quantum chemical modeling of ground states of CO 2 chemisorbed on anatase (001),(101), and (010) TiO 2 surfaces. *Energy & Fuels*, *22*(4), 2611-2618.

[14] Indrakanti, V. P., Kubicki, J. D., & Schobert, H. H. (2009). Photoinduced activation of CO 2 on Ti-based heterogeneous catalysts: Current state, chemical physics-based insights and outlook. *Energy & Environmental Science*, *2*(7), 745-758.

[15] Inoue, T., Fujishima, A., Konishi, S., & Honda, K. (1979). Photoelectrocatalytic reduction of carbon dioxide in aqueous suspensions of semiconductor powders. *Nature*, *277*(5698), 637-638.

[16] Izumi, Y. (2013). Recent advances in the photocatalytic conversion of carbon dioxide to fuels with water and/or hydrogen using solar energy and beyond. *Coordination Chemistry Reviews*, *257*(1), 171-186.

[17] Jacobson, M. Z. (2009). Review of solutions to global warming, air pollution, and energy security. *Energy & Environmental Science*, *2*(2), 148-173.

[18] Jiao, W., Wang, L., Liu, G., Lu, G. Q., & Cheng, H. M. (2012). Hollow anatase TiO2 single crystals and mesocrystals with dominant {101} facets for improved photocatalysis activity and tuned reaction preference. *Acs Catalysis*, *2*(9), 1854-1859.

[19] Kubacka, A., Fernandez-Garcia, M., & Colon, G. (2011). Advanced nanoarchitectures for solar photocatalytic applications. *Chemical Reviews*, *112*(3), 1555-1614.

[20] Kuznetsov, V. L., & Edwards, P. P. (2010). Functional materials for sustainable energy technologies: four case studies. *ChemSusChem*, *3*(1), 44-58.

[21] Lazzeri, M., & Selloni, A. (2001). Stress-driven reconstruction of an oxide surface: the anatase TiO 2 (001)−(1× 4) surface. *Physical review letters*, *87*(26), 266105.

[22] Lazzeri, M., Vittadini, A., & Selloni, A. (2001). Structure and energetics of stoichiometric TiO 2 anatase surfaces. *Physical Review B*, *63*(15), 155409.

[23] Li, P., Ouyang, S., Zhang, Y., Kako, T., & Ye, J. (2013). Surface-coordination-induced selective synthesis of cubic and orthorhombic NaNbO 3 and their photocatalytic properties. *Journal of Materials Chemistry A*, *1*(4), 1185-1191.

[24] Liao, Y., Cao, S. W., Yuan, Y., Gu, Q., Zhang, Z., & Xue, C. (2014). Efficient CO2 Capture and Photoreduction by Amine-Functionalized TiO2. *Chemistry-A European Journal*, *20*(33), 10220-10222.

[25] Lin, M. T., Occhialini, A., Andralojc, P. J., Devonshire, J., Hines, K. M., Parry, M. A., & Hanson, M. R. (2014). β-Carboxysomal proteins assemble into highly organized structures in Nicotiana chloroplasts. *The Plant Journal*, *79*(1), 1-12.

[26] Liu, G., Hoivik, N., Wang, K., & Jakobsen, H. (2012). Engineering TiO2 nanomaterials for CO2 conversion/solar fuels. *Solar Energy Materials and Solar Cells*, *105*, 53-68.

[27] Liu, G., Jimmy, C. Y., Lu, G. Q. M., & Cheng, H. M. (2011). Crystal facet engineering of semiconductor photocatalysts: motivations, advances and unique properties. *Chemical Communications*, *47*(24), 6763-6783.

[28] Liu, G., Niu, P., Sun, C., Smith, S. C., Chen, Z., Lu, G. Q., & Cheng, H. M. (2010). Unique electronic structure induced high photoreactivity of sulfur-doped graphitic C3N4. *Journal of the American Chemical Society*, *132*(33), 11642-11648.

[29] Liu, G., Yang, H. G., Wang, X., Cheng, L., Pan, J., Lu, G. Q., & Cheng, H. M. (2009). Visible light responsive nitrogen doped anatase TiO2 sheets with dominant {001} facets derived from TiN. *Journal of the American Chemical Society*, *131*(36), 12868-12869.

[30] Liu, J. Y., Garg, B., & Ling, Y. C. (2011). Cu x Ag y In z Zn k S m solid solutions customized with RuO 2 or Rh 1.32 Cr 0.66 O 3 co-catalyst display visible light-driven catalytic activity for CO 2 reduction to CH 3 OH. *Green Chemistry*, *13*(8), 2029-2031.

[31] Liu, L., Zhao, H., Andino, J. M., & Li, Y. (2012). Photocatalytic CO2 reduction with H2O on TiO2 nanocrystals: Comparison of anatase, rutile, and brookite polymorphs and exploration of surface chemistry. *Acs Catalysis*, *2*(8), 1817-1828.

[32] Liu, M., You, W., Lei, Z., Zhou, G., Yang, J., Wu, G., & Domen, K. (2004). Water reduction and oxidation on Pt–Ru/Y 2 Ta 2 O 5 N 2 catalyst under visible light irradiation. *Chemical communications*, (19), 2192-2193.

[33] Liu, Q., Low, Z. X., Li, L., Razmjou, A., Wang, K., Yao, J., & Wang, H. (2013). ZIF-8/Zn 2 GeO 4 nanorods with an enhanced CO 2 adsorption property in an aqueous medium for photocatalytic synthesis of liquid fuel. *Journal of Materials Chemistry A*, *1*(38), 11563-11569.

[34] Liu, Q., Zhou, Y., Kou, J., Chen, X., Tian, Z., Gao, J., & Zou, Z. (2010). High-yield synthesis of ultralong and ultrathin Zn2GeO4 nanoribbons toward improved photocatalytic reduction of CO2 into renewable hydrocarbon fuel. *Journal of the American Chemical Society*, *132*(41), 14385-14387.

[35] Liu, Q., Zhou, Y., Tian, Z., Chen, X., Gao, J., & Zou, Z. (2012). Zn 2 GeO 4 crystal splitting toward sheaf-like, hyperbranched nanostructures and photocatalytic reduction of CO 2 into CH 4 under visible light after nitridation. *Journal of Materials Chemistry*, *22*(5), 2033-2038.

[36] Lüthi, D., Le Floch, M., Bereiter, B., Blunier, T., Barnola, J. M., Siegenthaler, U., & Stocker, T. F. (2008). High-resolution carbon dioxide concentration record 650,000–800,000 years before present. *Nature*, *453*(7193), 379.

[37] Ma, Y., Wang, X., Jia, Y., Chen, X., Han, H., & Li, C. (2014). Titanium dioxide-based nanomaterials for photocatalytic fuel generations. *Chemical reviews*, *114*(19), 9987-10043.

[38] Moore, G. F., & Brudvig, G. W. (2011). Energy conversion in photosynthesis: a paradigm for solar fuel production. *Annu. Rev. Condens. Matter Phys.*, *2*(1), 303-327.

[39] Morris, A. J., Meyer, G. J., & Fujita, E. (2009). Molecular approaches to the photocatalytic reduction of carbon dioxide for solar fuels. *Accounts of Chemical Research*, *42*(12), 1983-1994.

[40] Nocera, D. G. (2012). The artificial leaf. *Accounts of Chemical Research*, *45*(5), 767-776.

[41] Paracchino, A., Laporte, V., Sivula, K., Grätzel, M., & Thimsen, E. (2011). Highly active oxide photocathode for photoelectrochemical water reduction. *Nature materials*, *10*(6), 456.

[42] Reece, S. Y., Hamel, J. A., Sung, K., Jarvi, T. D., Esswein, A. J., Pijpers, J. J., & Nocera, D. G. (2011). Wireless solar water splitting using silicon-based semiconductors and earth-abundant catalysts. *Science*, *334*(6056), 645-648.

[43] Roy, S. C., Varghese, O. K., Paulose, M., & Grimes, C. A. (2010). Toward solar fuels: photocatalytic conversion of carbon dioxide to hydrocarbons. *Acs Nano*, *4*(3), 1259-1278.

[44] Smith, A. M., & Nie, S. (2009). Semiconductor nanocrystals: structure, properties, and band gap engineering. *Accounts of chemical research*, *43*(2), 190-200.

[45] Tahir, M., & Amin, N. S. (2013). Advances in visible light responsive titanium oxide-based photocatalysts for CO2 conversion to hydrocarbon fuels. *Energy Conversion and Management*, *76*, 194-214.

[46] Tong, H., Ouyang, S., Bi, Y., Umezawa, N., Oshikiri, M., & Ye, J. (2012). Nano-photocatalytic materials: possibilities and challenges. *Advanced materials*, *24*(2), 229-251.

[47] Truong, Q. D., Le, T. H., Liu, J. Y., Chung, C. C., & Ling, Y. C. (2012). Synthesis of TiO2 nanoparticles using novel titanium oxalate complex towards visible light-driven photocatalytic reduction of CO2 to CH3OH. *Applied Catalysis A: General*, *437*, 28-35.

[48] Truong, Q. D., Liu, J. Y., Chung, C. C., & Ling, Y. C. (2012). Photocatalytic reduction of CO2 on FeTiO3/TiO2 photocatalyst. *Catalysis Communications*, *19*, 85-89.

[49] Varghese, O. K., Paulose, M., LaTempa, T. J., & Grimes, C. A. (2009). High-rate solar photocatalytic conversion of CO2 and water vapor to hydrocarbon fuels. *Nano letters*, *9*(2), 731-737.

[50] Vittadini, A., Selloni, A., Rotzinger, F. P., & Grätzel, M. (1998). Structure and energetics of water adsorbed at TiO 2 anatase\(101\) and\(001\) surfaces. *Physical Review Letters*, *81*(14), 2954.

[51] Wang, W. S., Wang, D. H., Qu, W. G., Lu, L. Q., & Xu, A. W. (2012). Large ultrathin anatase TiO2 nanosheets with exposed {001} facets on graphene for enhanced visible light photocatalytic activity. *The Journal of Physical Chemistry C*, *116*(37), 19893-19901.

[52] Wang, W., Dahl, M., & Yin, Y. (2012). Hollow nanocrystals through the nanoscale Kirkendall effect. *Chemistry of Materials*, *25*(8), 1179-1189.

[53] Wang, W., Dahl, M., & Yin, Y. (2012). Hollow nanocrystals through the nanoscale Kirkendall effect. *Chemistry of Materials*, *25*(8), 1179-1189.

[54] Wu, B., Guo, C., Zheng, N., Xie, Z., & Stucky, G. D. (2008). Nonaqueous production of nanostructured anatase with high-energy facets. *Journal of the American Chemical Society*, *130*(51), 17563-17567.

[55] Xi, G., Ouyang, S., Li, P., Ye, J., Ma, Q., Su, N., & Wang, C. (2012). Ultrathin W18O49 Nanowires with Diameters below 1 nm: Synthesis, Near-Infrared Absorption, Photoluminescence, and Photochemical Reduction of Carbon Dioxide. *Angewandte Chemie International Edition*, *51*(10), 2395-2399.

[56] Yang, C. C., Yu, Y. H., van der Linden, B., Wu, J. C., & Mul, G. (2010). Artificial photosynthesis over crystalline TiO2-based catalysts: fact or fiction?. *Journal of the American Chemical Society*, *132*(24), 8398-8406.

[57] Yang, H. G., Sun, C. H., Qiao, S. Z., Zou, J., Liu, G., Smith, S. C., & Lu, G. Q. (2008). Anatase TiO 2 single crystals with a large percentage of reactive facets. *Nature*, *453*(7195), 638.

[58] Yang, N., Zhai, J., Wang, D., Chen, Y., & Jiang, L. (2010). Two-dimensional graphene bridges enhanced photoinduced charge transport in dye-sensitized solar cells. *ACS nano*, *4*(2), 887-894.

[59] Yu, J., Fan, J., & Zhao, L. (2010). Dye-sensitized solar cells based on hollow anatase TiO2 spheres prepared by self-transformation method. *Electrochimica Acta*, *55*(3), 597-602.

[60] Yu, J., Low, J., Xiao, W., Zhou, P., & Jaroniec, M. (2014). Enhanced photocatalytic CO2-reduction activity of anatase TiO2 by coexposed {001} and {101} facets. *Journal of the American Chemical Society*, *136*(25), 8839-8842.

[61] Yui, T., Kan, A., Saitoh, C., Koike, K., Ibusuki, T., & Ishitani, O. (2011). Photochemical reduction of CO2 using TiO2: effects of organic adsorbates on TiO2 and deposition of Pd onto TiO2. *ACS applied materials & interfaces*, *3*(7), 2594-2600.